Author post-print

IEEE Transactions on Microwave Theory and Techniques,
Volume: 65, Issue: 5, pp. 1397 - 1406, May 2017

A hybrid Crank-Nicolson FDTD subgridding boundary condition for lossy thin-layer modeling

M. R. Cabello[1], L. D. Angulo[1], J. Alvarez[2], I. D. Flintoft[3], S. Bourke[3] and J. Dawson[3]

[1]*Department of Electromagnetism, University of Granada, Fuentenueva, Granada, Spain*
[2]*Airbus Defence and Space, Avd. John Lennon, Getafe, Spain*
[3]*Department of Electronics, University of York, Heslington, York YO10 5DD, UK*

Accepted for publication in IEEE Transaction on Microwave Theory and Techniques

Accepted for publication 04/12/2016

DOI: 10.1109/TMTT.2016.2637348

A hybrid Crank-Nicolson FDTD subgridding boundary condition for lossy thin-layer modeling

M. R. Cabello[1], L. D. Angulo[1], J. Alvarez[2], *Member IEEE*, I. D. Flintoft[3], *Senior Member, IEEE*, S. Bourke[3], J. Dawson[3], *Member IEEE*, R. G. Martin[1] and S. G. Garcia[1], *Senior Member IEEE*

***Abstract*—The inclusion of thin lossy, material layers, such as carbon based composites, is essential for many practical applications modeling the propagation of electromagnetic energy through composite structures such as those found in vehicles and electronic equipment enclosures. Many existing schemes suffer problems of late time instability, inaccuracy at low frequency, and/or large computational costs. This work presents a novel technique for the modeling of thin-layer lossy materials in FDTD schemes which overcomes the instability problem at low computational cost. For this, a 1D-subgrid is used for the spatial discretization of the thin layer material. To overcome the additional time-step constraint posed by the reduction in the spatial cell size, a Crank-Nicolson time-integration scheme is used locally in the subgridded zone, and hybridized with the usual 3D Yee-FDTD method, which is used for the rest of the computational domain. Several numerical experiments demonstrating the accuracy of this approach are shown and discussed. Results comparing the proposed technique with classical alternatives based on impedance boundary condition approaches are also presented. The new technique is shown to have better accuracy at low frequencies, and late time stability than existing techniques with low computational cost.**

***Index Terms*—Finite-Difference Time Domain (FDTD), sub-cell models, thin layers, Crank-Nicolson, hybrid implicit-explicit (HIE), Carbon fiber composite, Electromagnetic shielding, Lossy materials**

I. Introduction

THE accurate treatment of lossy thin layers is a must in electromagnetic simulation tools as many vehicles and enclosures contain them for electromagnetic or structural reasons. Examples include: carbon fiber layers [1], metal meshes [2], carbon nanotube [3] or graphene loaded composites [4], and metalised coatings [5]. Also propagation through joints and small apertures presents similar problems [6]. The 3D modeling of lossy layers, joints and small apertures is usually avoided for being unaffordable in terms of computational cost, making sub-cell models the preferred approach. In the context of Finite Difference Time Domain (FDTD) methods [7], three main techniques are found: i) equivalent-parameter models; ii) Leontovich-based Impedance Boundary Conditions; and iii) fine-mesh discretization.

Equivalent parameter (EP) models [8] have been demonstrated to accurately predict the conductive properties of electrically thin panels at low frequencies (LF). These models are based on the definition of average constitutive parameters used to update the tangential E-field components at the slab interfaces . They can model arbitrary dispersive behavior [9], and use extra degrees-of-freedom, to handle the discontinuity in the normal components. These models are accurate for frequencies where the slab thickness is smaller than, or comparable to the skin depth. Leontovich-based [10] Network Impedance Boundary Conditions (NIBC) constitute a widely used alternative [1], [11] for high frequencies (HF) where the EP approximation fails. NIBC techniques assume plane-wave propagation inside the slab, along the direction normal to its surface, which is a reasonable hypothesis for highly conductive media with a refractive index much higher than that of the surrounding media. In this manner, NIBC does not need to take into account field components that are normal to the slab and only finds the tangential electric and magnetic fields at each slab interface by frequency-domain matrix impedance relationships. The time-domain implementation in FDTD can be made in a number of ways: piecewise linear recursive convolution (PLRC) [11], auxiliary differential equation algorithms [12], circuital equivalents [6], [13], etc.. A drawback of NIBC methods usually reported in literature for FDTD resides in the appearance of late-time instabilities [4], [14], whose origin is still not well understood.

Finally, a natural alternative to EP and NIBC is the use of a dense spatial discretization inside the layer to properly resolve the wavelength inside it, thus allowing us to accurately deal with LF and HF regimes. In this paper, we adopt such an approach combined with an unconditionally stable Crank-Nicolson Time-Domain method (CNTD) [15]. CNTD allows us to overcome the reduction in the time step (for stability) enforced by the reduction in the space step, if the usual FDTD Yee scheme, or an exponential time differencing one [16], were employed instead. A hybrid implicit-explicit (HIE) algorithm [17] is used to combine the CNTD method inside the slab with the usual 3D Yee-FDTD method used outside it.

To this end, we start in Section II-A from the same assumption of a plane wave propagating only in the direction normal to the slab surface, as used for the NIBC. Next, in Section II-B, instead of finding the E and H tangential components on either side of the slab by impedance relationships, they are found by

[1] Dept. of Electromagnetism, University of Granada, Fuentenueva s/n, 18071 Granada, Spain (e-mail: {mcabello,lmdiazangulo,arubio,rgomez,salva}@ugr.es). [2]Airbus Defence and Space, Avd. John Lennon s/n, 28906 Getafe, Spain (e-mail: jesus.g.alvarez@airbus.com). [3]Department of Electronics, University of York, York YO10 5DD, U.K. (e-mail {ian.flintoft,samuel.bourke,john.dawson}@york.ac.uk)

This work has received funding from the Projects TEC2013-48414-C3-01, TEC2016-79214-C3-3-R, and TEC2015-68766-REDC (Spanish MINECO, EU FEDER), P12-TIC-1442 (J. de Andalucia, Spain), Alhambra-UGRFDTD (AIRBUS DS), and by the CSIRC alhambra.ugr.es supercomputing center. This work was also supported by a STSM Grant from COST Action IC1407 (ACCREDIT)

the 1D time-stepping algorithm which explicitly propagates the fields inside the slab. The slab is meshed in its normal direction with a space step finer than the one used in the surrounding medium, chosen to keep a minimum resolution in the slab of about 10 cells per wavelength at the maximum frequency. The tangential E-field components lying at the boundaries between the 1D and the 3D domain are updated by using a weighted average conductivity and permeability. The resulting algorithm can be regarded as a sub-gridding boundary condition (SGBC), and a robust and computationally affordable alternative to NIBC both for HF and LF problems.

In Section III-A and III-B, the stability and accuracy of the different SGBC algorithms is analyzed. In Section IV, a validation is performed in two different scenarios: for shielding-effectiveness prediction in HF, and for resistance prediction in LF conductive problems.

II. Alternatives for thin-panel modeling

A. Impedance Boundary Condition

Let us assume that a plane wave impinges on a conductive planar slab with oblique incidence. If the refractive index is much higher inside the slab than outside, refracted waves travel inside the slab at a close-to-normal angle $\theta_t \to 0$ regardless of the actual angle of incidence θ_i. For instance for a lossy medium with free-space permittivity, embedded in free-space, Snell's law can be written as:

$$\sin(\theta_t) = \sin(\theta_i)/\sqrt{1 - j/Q}\ ,\ Q = 2\pi f \tau\ ,\ \tau = \frac{\varepsilon}{\sigma} \tag{1}$$

where Q is the quality factor, τ is the relaxation time constant, and σ is the conductivity of the medium. For instance, for grazing incidence as $\theta_i \to \pi/2$ (the worst-case), we find that $|\theta_t| < 10^{-2}$ if

$$f\,[\mathrm{GHz}] < 1.8\,\sigma\,(\mathrm{kS/m}) \tag{2}$$

For instance, for conductivities of $\sigma > 10^4\,\mathrm{S/m}$, the applicability of the model is up to 18 GHz, regardless of the thickness of the slab. Therefore, the transverse plane-wave assumption enables us to make a general analysis of most common slab conductive materials in automotive or aeronautics applications.

The S-parameters of the slab can be determined analytically if its frequency-dependent constitutive parameters are known, or they can be determined from modelling or measurement. From the S parameters, the two-port network Z-parameters relating the electric and magnetic field components of the transverse plane wave on either side of the slab can be found [18]. For instance, if we consider an isotropic slab, the fields E_S, H_S on each side are related by:

$$\begin{bmatrix} E_{S1} \\ E_{S2} \end{bmatrix} = \underbrace{\begin{bmatrix} Z_{11} & Z_{12} \\ Z_{21} & Z_{22} \end{bmatrix}}_{\tilde{Z}(\omega)} \begin{bmatrix} H_{S1} \\ -H_{S2} \end{bmatrix} \tag{3}$$

where E_{S1} and H_{S1} are the fields on one side of the slab and E_{S2} and H_{S2} are the fields on the other. A similar relation exists for E_S, H_S. $Z_{12} = Z_{21}$ for reciprocal media, and $Z_{11} = Z_{22}$ for left-to-right symmetric media. This model can be generalized for multilayered anisotropic media [1], [11] by cascading the ABCD parameters of the four-port network model of each layer, to find a 4×4 Z-relationship similar to (3).

The NIBC technique [1], [11] employs the relationship (3) to relate the fields on either side of the slab, which serve in turn as boundary conditions for the 3D Yee-FDTD scheme used for the rest of the problem. For this, the frequency-domain relationship (3) is typically cast into the time domain (TD) by firstly expanding each term of matrix $\tilde{Z}$ into a sum of partial fractions found by a vector-fitting (VF) procedure [19]

$$\tilde{Z}(\omega) = \tilde{Z}_\infty + \sum_{k=1}^{P} \frac{\tilde{r}_k}{j\omega - p_k} \tag{4}$$

Next, a TD numerical relationship can be found in several ways [6], [11]–[13], [20]. In this paper, we compare the results of our SGBC with the Digital Filter (DigFilt) representation of the NIBC [6], which employs a face-centered formulation. The resulting model is both causal (automatically complies with Kramers-Kronig relationships), and stable (poles are in the left complex semi-plane).

The main drawback of NIBC is its requirement to simultaneously know both the E and H-fields at the same point on the interface. Since FDTD does not co-locate these components in space-time, NIBC typically extrapolates the H-field from half a cell away [11], and half a time-step before, which is actually a 0^{th}-order approximation to the field at the interface. This extrapolation is typically cited as being one main reason for the appearance of late-time instabilities, and several efforts to overcome it have been published [4], [14]. From our experience, even if canonical problems do not suffer from late-time instabilities, large and complex ones do exhibit them when using the same NIBC model. A typical workaround to remove instabilities is the reduction of the time-step in an iterative heuristic way hopefully concluding with a computationally affordable model. This issue limits the applicability of the method.

B. Subgridding boundary condition

Subgridding techniques are widely employed in FDTD [21], [22], particularly to treat composite materials [23]. Subgridding is typically considered a brute-force method, yielding restrictive stability conditions that may become prohibitive. In this paper, we present a new HIE SGBC, inspired by the NIBC described above. It combines a 1D FDTD scheme to deal with fields inside the slab, with the usual 3D Yee-FDTD scheme for the rest of the problem. For this, the same starting principle used for NIBC is considered: thin-panel with a planar shape and plane waves propagating inside it at a normal angle.

However, instead of the impedance relationships (3) used by NIBC to find the fields on both faces of the panel, SGBC finds them after a full-wave 1D simulation inside the slab, which is meshed into a fine spatial mesh, only along the direction normal to the panel, with a high enough number of cells to properly resolve the wavelength and the skin-depth at the maximum frequency of interest inside the slab.

To overcome the drawback posed by the reduced time-step required for the stability of the overall FDTD scheme,

a novel approach based on a CNTD unconditionally stable scheme is employed. The E and H fields inside the slab are advanced by the 1D CNTD method, which is tridiagonally implicit in 1D [24] and has a small computational overhead, compared with FDTD. This is more than compensated for by its unconditionally stable nature, which means that we do not need to reduce the time step in the entire space, which would be the case if a classical 1D Yee-FDTD were applied in the slab region.

We will next illustrate the CNTD and SGBC algorithms with the geometry depicted in Fig. 1. In this case, the thin slab has been sub-gridded into N 1D-cells of size Δ_{fine}, with $N+1$ E-field and N H-field components inside. For simplicity the surrounding medium is assumed to be free space with a 3D cell size Δ_{coarse}, and the slab is assumed to have free-space permittivity, and a constant conductivity.

C. Hybrid 1D CNTD - 3D FDTD

Let first describe the 1D CNTD used inside the thin slab shown in Fig. 1 (fuller details of CNTD can be found in several places, e.g., [25]). For this, we start from the usual Yee-FDTD equations for the Ampere-Maxwell law, assuming that H-fields are located at integer time-steps and using a time average for the right-hand-side E-fields to also co-locate them in time with the H-field components

$$H_{L,i+1/2}^{n+1} = D_{a,i+1/2} H_{L,i+1/2}^{n} + \frac{D_{b,i+1/2}}{2}\left(E_{L,i}^{n} - E_{L,i+1}^{n} + E_{L,i}^{n+1} - E_{L,i+1}^{n+1}\right) \tag{5}$$

Using the same method for Faraday's law, we find

$$E_{L,i}^{n+1} = C_{a,i} E_{L,i}^{n} + \frac{C_{b,i}}{2}\left(H_{L,i-1/2}^{n+1} - H_{L,i+1/2}^{n+1} + H_{L,i-1/2}^{n} - H_{L,i+1/2}^{n}\right) \tag{6}$$

where we use the well-known notation for the material constants $C_{a,i}, C_{b,i}, D_{a,i+1/2}, D_{b,i+1/2}$ from [22] for lossy electric, lossless magnetic media

$$C_{a,i} = \frac{2-\Delta t/\tau_i}{2+\Delta t/\tau_i}\,,\; C_{b,i} = \frac{2\Delta t/(\varepsilon_i \Delta_{\text{fine},i})}{2+\Delta t/\tau_i}\,,\; \tau_i = \frac{\varepsilon_i}{\sigma_i}$$
$$D_{a,i+1/2} = 1\,,\; D_{b,i+1/2} = \frac{\Delta t}{\mu_i \Delta_{\text{fine},i+1/2}} \tag{7}$$

Now extracting H^{n+1} from (5) and inserting it into (6), a fully consistent algorithm with the space positions of E and H staggered in space as in the usual Yee-Scheme is yielded, but evaluated at co-located integer time-steps. After some algebra, a tridiagonal system of equations is found for the E-fields for $i = 2, \ldots, N$

$$a_i E_{L,i-1}^{n+1} + b_i E_{L,i}^{n+1} + c_i E_{L,i+1}^{n+1} = d_i^n \tag{8}$$

where coefficients a_i, b_i, c_i, d_i are given in the Appendix. With a back-substitution algorithm used to solve the tridiagonal system, all $E_{L,i}^{n+1}$ are found. Inserting them into (5) , the magnetic field components can be finally found in an explicit manner.

Next, a proper HIE scheme has been devised to connect the solutions found by CNTD (inside the slab) and by Yee-FDTD (outside the slab). For this, we assume that the CNTD-domain is terminated in the E-field components E_{S1} and E_{S2}, and we modify the CNTD procedure found after (6), so that only the H-fields inside the CNTD-domain are averaged in time, while those outside are those previously found by the usual Yee-FDTD at semi-integer time-steps, thus playing the role of external source terms. Hence, for the $(L,1)$, $(L,N+1)$ boundaries, we find

$$E_{L,1}^{n+1} = C_{a,1} E_{L,1}^{n} + C_{b,1}\left(H_{S1}^{n+1/2} - \frac{H_{L,3/2}^{n} + H_{L,3/2}^{n+1}}{2}\right) \tag{9a}$$

$$E_{L,N+1}^{n+1} = C_{a,N+1} E_{L,N+1}^{n} + C_{b,N+1}\left(\frac{H_{L,N+1/2}^{n} + H_{L,N+1/2}^{n+1}}{2} - H_{S2}^{n+1/2}\right) \tag{9b}$$

To account for the different space steps and different materials on either side of the boundary, the constants $C_{a,1}, C_{a,N+1}, C_{b,1}, C_{b,N+1}$ are evaluated in (7) by employing the effective constitutive parameters ε_i and σ_i found by using the integral versions of Maxwell's equations [22]

$$\sigma_i = \frac{\sigma_{i-1/2}\Delta_{\text{fine},i-1/2} + \sigma_{i+1/2}\Delta_{\text{fine},i+1/2}}{\Delta_{\text{fine},i-1/2} + \Delta_{\text{fine},i+1/2}}$$
$$\varepsilon_i = \frac{\varepsilon_{i-1/2}\Delta_{\text{fine},i-1/2} + \varepsilon_{i+1/2}\Delta_{\text{fine},i+1/2}}{\Delta_{\text{fine},i-1/2} + \Delta_{\text{fine},i+1/2}} \tag{10}$$

where $\Delta_{\text{fine,1/2}} = \Delta_{\text{coarse}}$ and $\Delta_{\text{fine,N+3/2}} = \Delta_{\text{coarse}}$.

Inserting the magnetic fields inside the slab found by CNTD by (5) into (9), we get two implicit equations that must be solved together with (8) for the interior E-fields

$$b_1 E_{L,1}^{n+1} + c_1 E_{L,2}^{n+1} = d_1^n \tag{11a}$$

$$a_{N+1} E_{L,N}^{n+1} + b_{N+1} E_{L,N+1}^{n+1} = d_{N+1}^n \tag{11b}$$

where the modified coefficients $a_1, c_1, a_{N+1}, b_{N+1}, d_1^n, d_{N+1}^n$ are also given in the Appendix. The above procedure permits us a consistent connection between CNTD and Yee-FDTD in such a way that the CNTD algorithm employs only the 3D Yee-FDTD H-fields as source terms, this means that the unconditional stability of the CNTD algorithm is not degraded, even if the surrounding media is also conductive [26], as later shown.

D. SGBC algorithm

As in the NIBC, the SGBC duplicates the tangential E-fields on the slab surface E_{S1}, E_{S2} to account for each face value. They are located at the usual staggered space-time indexes of the Yee-FDTD cell. Also, as usual, the H-fields are located at the center of the adjacent 3D cells H_{S1}, H_{S2}. The SGBC algorithm is as follows:

1) The fields inside the slab domain denoted by $E_{L,i}^{n}$, $H_{L,i+1/2}^{n}$ see Fig. 1 are updated by the usual 1D CNTD described above.
2) E-fields outside the slab are advanced $\vec{E}^{n}$ in the usual 3D Yee-FDTD manner.
3) H-fields outside the slab are advanced $\vec{H}^{n+1/2}$ in the usual 3D Yee-FDTD manner.

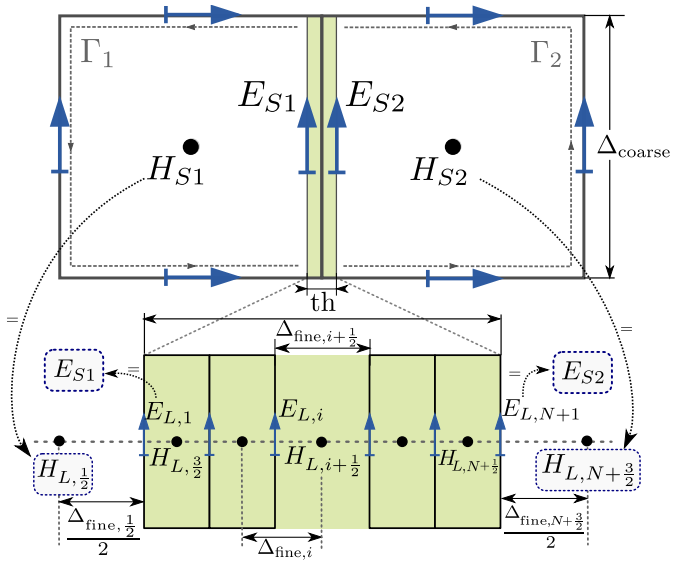

Fig. 1. Cross section of a FDTD cell with a SGBC boundary.

4) H-fields at the adjacent cells $H_{S1}^{n+1/2}$ and $H_{S2}^{n+1/2}$, employ the usual 3D algorithm with $E_{S1}^n = E_{L,1}^n$ and $E_{S2}^n = E_{L,N+1}^n$

$$H_{S1}^{n+1/2} = H_{S1}^{n-1/2} - \frac{\Delta t}{\mu_0 A_1}\left(\Gamma_1^n + \Delta_{\text{coarse}}\ E_{S1}^n\right)$$
$$H_{S2}^{n+1/2} = H_{S2}^{n-1/2} - \frac{\Delta t}{\mu_0 A_2}\left(\Gamma_2^n - \Delta_{\text{coarse}}\ E_{S2}^n\right) \quad (12)$$

Where $\Gamma_j^n = \sum_{\text{cell}j} \Delta_i E_i^n$ is the usual discrete line integral of the E-field components along the 3 non-boundary edges. The surfaces used for the flux of the H-field are corrected to take into account the slab thickness $A_{1,2} = \Delta_{\text{coarse}}\left(\Delta_{\text{coarse}} - \frac{th}{2}\right)$.

5) The connection between the coarse (Yee) and fine (CNTD) mesh is made through the tangential electric field on the slab surface, which is found by the HIE algorithm described above.

This method can be easily extended for arbitrary frequency dispersion, by finding equivalent single-layer electric and magnetic dispersive models [27]. The CNTD method can also be easily extended to handle these media, for instance by employing the formulation of [28]. Anisotropic panels could also be handled by unconditionally stable split-step methods [33].

III. Numerical Characteristics of SGBC

A. Stability

The CNTD method is well known for being unconditionally stable [29]. By using a heuristic procedure, we have shown that the stability condition is kept unaltered by the HIE CNTD-FDTD scheme, with respect to the usual one

$$c^2\Delta t^2 \leq 1/(\Delta x^{-2} + \Delta y^{-2} + \Delta z^{-2}) \quad (13)$$

Fig. 2 shows the stability analysis for the method described in this paper, compared to the one that would be enforced if using a 1D Yee-FDTD scheme, instead of the 1D CNTD one. The stability limit is unaltered for the lossy case with respect to the usual lossless one for the usual time-average scheme [26]. In the lower x-axis the inverse of the Q-factor at the frequency of interest is shown $1/Q = \sigma/(\omega\varepsilon_0)$. In the y-axis the maximum Courant-Friedrichs-Lewy number (CFLN) in the coarse region (CFLN=$c\Delta t/\Delta_{\text{coarse}}$ for the 1D case is shown to achieve a constant space resolution in the lossy slab $\lambda_{\text{slab}}/\Delta_{\text{fine}} = 10$ (equal to that used in free space at that frequency $\lambda_{\text{air}}/\Delta_{\text{coarse}} = 10$). The upper x-axis provides a means to calculate the space step at the fine region Δ_{fine} to have a resolution of 10 cells/λ_{slab} for a given $1/Q$ factor. Notice that for most practical problems $1/Q > 10^5$ with typical slabs of $h >$ 1mm the slab becomes a PEC in practice and subgriddings $\Delta_{\text{coarse}}/\Delta_{\text{fine}} > 64$ become useless since penetration is negligible.

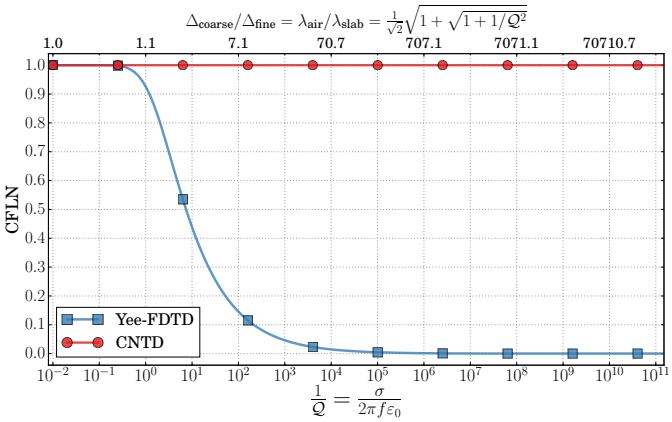

Fig. 2. Maximum 1D CFLN in the coarse region for stability for the different SGBC schemes. The space steps are fixed to keep a constant space resolution in free space $\lambda_{\text{air}}/\Delta_{\text{coarse}} = 10$ equal to that in the lossy slab $\lambda_{\text{slab}}/\Delta_{\text{fine}} = 10$.

A key aspect for the robust stability of SGBC resides in the fact that the HIE algorithm just connects the Yee-FDTD and the CNTD regions by means of boundary conditions, with no other interpolation/extrapolation procedure.

B. Accuracy

Non-physical reflections are well known to be produced at boundaries between subgridded regions [30]. In this section, we study this error with two different test setups.

In the first one an infinite reflectionless (free-space) planar slab, with a different mesh from its surrounding free space, is illuminated with a plane wave normally incident. Fig. 4 shows the reflection coefficient (ideally zero) and transmission coefficient (ideally unity) for SGBC-CNTD and SGBC-Yee-FDTD as a function of $\Delta_{\text{coarse}}/\Delta_{\text{fine}}$. The number of points per wavelength (PPW) in the slab, PPW_{fine}, is also shown for reference in the upper x-axis. The coefficients have been computed using a resolution outside the slab of $\text{PPW}_{\text{coarse}} = 100$ cells/wavelength. The effect of the backward wave created by the impressed source is removed by subtracting it from a first simulation without the slab. It bears noting that there is full reflection beneath the Nyquist limit $\text{PPW}_{\text{fine}} = 2$. Above the Nyquist limit the reflection coefficient decreases and, as

expected, becomes zero as for the usual Yee-FDTD when there is no jump in the discretization ($\Delta_{\text{coarse}}/\Delta_{\text{fine}} = 1$). When SGBC-CNTD is used instead, the error is not zero since numerical reflections appear at the interface between the CNTD and the Yee-FDTD scheme. When the discretization inside and outside coincide, the error begins to become constant, even for finer discretizations inside the slab, since it is dominated by the constant discretization outside it.

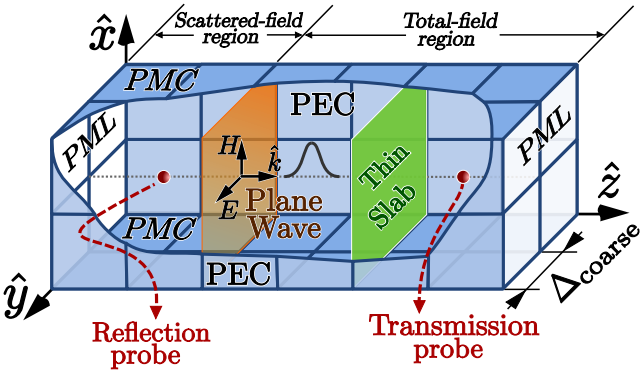

Fig. 3. Details of the test-setup for a uniform normally incident plane wave on a thin slab.

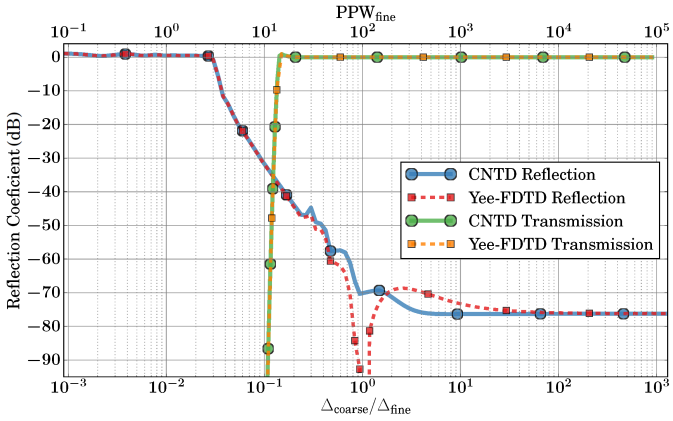

Fig. 4. Reflection and transmission coefficients (S_{11} and S_{12}) simulated for a uniform normally incident plane wave on a free-space slab for $\text{PPW}_{\text{coarse}} = 100$ fixed. Note that we keep the convention of Δ_{fine} for the space step inside the slab even for $\Delta_{\text{coarse}}/\Delta_{\text{fine}} < 1$ for which the discretization outside is actually finer than that inside.

An identical test setup has also been analyzed using a conductive slab instead of a free-space one. Fig. 5 shows the relative error for the SGBC-CNTD algorithm in the transmission coefficient as a function of PPW_{fine} for several values of $\text{PPW}_{\text{coarse}}$. The slab is chosen with $1/Q = 10^3$ and a thickness of 1 wavelength (roughly 2π times the skin-depth). As for the free-space case, we observe that the error trend becomes constant, dominated by the smallest PPW (coarse or fine).

C. Computer requirements

The computational overburden of the subcell method employed to deal with thin slabs has been studied by Amdahl's law (14). For this, we take into account the number of floating point operations (FLOPs) added by the subcell algorithm and

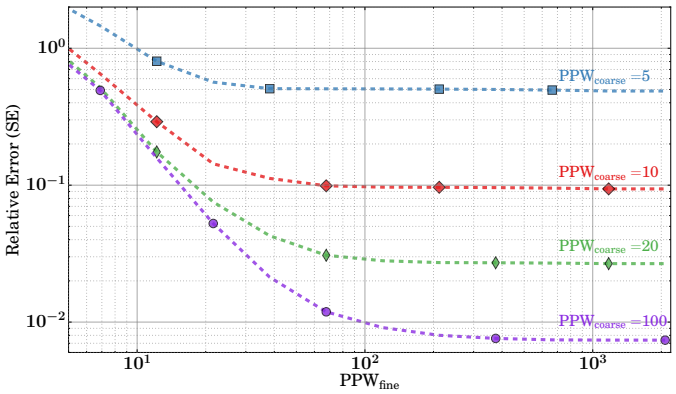

Fig. 5. Error in the shielding effectiveness ($SE = S_{12}^{-1}$) for a uniform normally incident plane wave on a conductive slab for SGBC-CNTD using several coarse resolutions. This error is found by $|\text{SE}_{\text{sim}} - \text{SE}_{\text{teo}}|/\text{SE}_{\text{teo}}$, with SE_{sim} and SE_{teo} being the simulation and analytical values.

compute the next figure-of-merit to measure the computer speed reduction

$$S = \frac{1}{(1 - N_{\text{cells}}) + \frac{N_{\text{cells}}}{A^{\text{FLOP}}}} \tag{14}$$

where N_{cells} is the ratio of sub-cell special cells to the total number of cells, and A^{FLOP} is the ratio of the number of FLOPs required by the usual FDTD with and without cells affected by the sub-cell treatment

$$A^{\text{FLOP}} = A^{\text{FLOP}}_{\text{FDTD}} / \left(A^{\text{FLOP}}_{\text{FDTD}} + A^{\text{FLOP}}_{\text{sub-cell}}\right) \tag{15}$$

For FDTD $A^{\text{FLOP}}_{\text{FDTD}} = 14$ (8 additions/substractions and 6 multiplications) and $A^{\text{FLOP}}_{\text{sub-cell}}$ depends on the number of new degrees-of-freedom added to the full problem: the number of layers for SGBC N_L, and the number of poles/residues N_p for NIBC (Table I).

TABLE I
$A^{\text{FLOP}}_{\text{SUB-CELL}}$ FOR THE DIFFERENT SUB-CELL METHODS.

Method	+ and -	*	/
SGBC with Yee-FDTD	$5 + 6\,N_L$	$4 + 4\,N_L$	0
SGBC with CNTD	$2 + 7\,N_L$	$2 + 5\,N_L$	$2 + 2\,N_L$
NIBC	$6 + 4\,N_p$	$4 + 12\,N_p$	0

In Fig. 6, we show the parameter defined in (14) as a function of N_L, and N_p for two different ratios of cells requiring a sub-cell treatment. Though N_L, and N_p are not magnitudes that can be compared, Fig. 6 can be used to provide an idea of the computational cost of each model for a certain performance degradation. For instance a $N_L = 22$ layers SGBC CNTD model requires the same number of FLOPS as a $N_p = 19$ model with SIBC, with a degradation in performance of $S = 0.9$ for 0.5% sub-cell cells and $S = 0.525$ for 4% sub-cell cells. These curves are ideal results which agree with data found after actual numerical simulations for small problems that can fit into memory caches. However, for large, problems the memory access time is actually dominant over the FLOP/second processor capabilities in the computational time of FDTD methods [31], and the CNTD and NIBC

curves tend to be closer. Finally let us also stress, that the apparent lower computer time requirement for the NIBC is obscured by its lack of robustness in stability, as mentioned in the introduction. This often requires reductions in the CFLN which are not necessary in the SGBC CNTD.

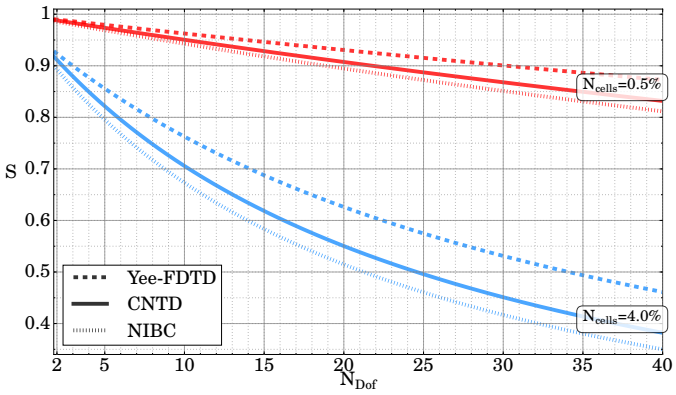

Fig. 6. S figure of merit. N_{Dof} stands either for N_L or N_p depending on the technique used.

IV. Validation

In this section, we show some canonical validations of this method for two cases of interest: the prediction of the shielding effectiveness of planar slabs, in scattering problems; and the LF resistance, which is of interest in conduction problems. Let us start by recalling the basic formulas.

A. Shielding effectiveness and DC resistance

The shielding effectiveness of an infinite planar slab under transverse plane-wave incidence, embedded in a medium with intrinsic impedance η_0 can be expressed from (3) as

$$SE = S_{12}^{-1} = \frac{(\eta_0 + Z_{11})(\eta_0 + Z_{22}) - Z_{12}^2}{2\eta_0 Z_{21}} \tag{16}$$

For instance, for a constant-conductivity slab of thickness h

$$\tilde{Z}(\omega) = \frac{\eta}{\sinh(\gamma h)} \begin{bmatrix} \cosh(\gamma h) & 1 \\ 1 & \cosh(\gamma h) \end{bmatrix} \tag{17}$$

with η the usual intrinsic impedance and with γ the wave propagation constant inside the slab. From this, the shielding effectiveness (16) can be expressed as

$$\text{SE} = \cosh(\gamma h) + \frac{1}{2}\left(\frac{\eta_0}{\eta} + \frac{\eta}{\eta_0}\right)\sinh(\gamma h) \tag{18}$$

The Z relationship (3) can also be used to find the resistance in the low-frequency limit for conductive media $Q \ll 1$

$$\tilde{Z}_{LF}(\omega) = \frac{\gamma}{\sigma \sinh(\gamma h)} \begin{bmatrix} 1 & 1 \\ 1 & 1 \end{bmatrix} \tag{19}$$

For instance, for a strip with width w and length l (Fig. 11), we can assume

$$E_{S1} = E_{S2} = \gamma \frac{H_{S1} - H_{S2}}{\sigma \sinh(\gamma h)} \tag{20}$$

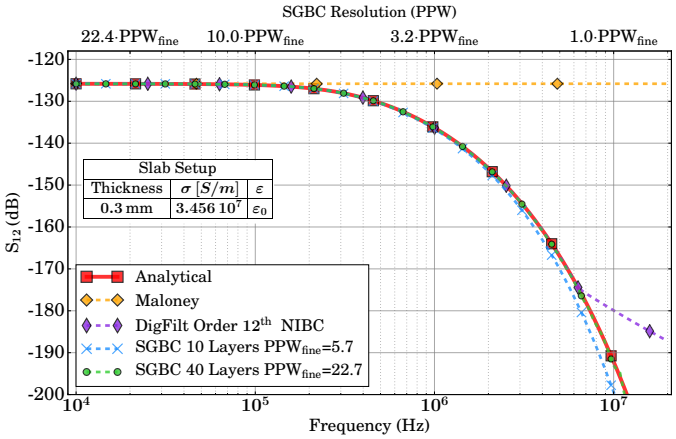

Fig. 7. $S_{12} = \text{SE}^{-1}$ for an aluminum planar slab with a conductivity $\sigma = 3.456 \cdot 10^7$ S/m and a thickness th $= 0.3$ mm. Space step $\Delta_{\text{coarse}} = 2.5$ mm.

and using a square Ampère path around it, the low-frequency impedance for the strip Z_t is

$$Z_t = \frac{\int_0^l \vec{E} \cdot \vec{dl}}{\int_S \vec{J} \cdot \vec{dS}} = \frac{\int_0^l \vec{E} \cdot \vec{dl}}{\oint_L \vec{H} \cdot \vec{dl}} = \frac{E_{S1} l}{w(H_{S1} - H_{S2})} = \frac{\gamma h}{\sinh(\gamma h)} R_{DC} \tag{21}$$

with R_{DC} the resistance, usually found from Ohm's law $R_{DC} = \frac{l}{w\sigma h}$. For thin-slabs $\gamma h \ll 1$, highly conductive ($\eta \simeq \frac{\gamma}{\sigma} \ll \eta_0$), and at the DC limit ($\omega \to 0$) , we can further simplify

$$Z_t \simeq \frac{l\eta_0}{2w}\frac{1}{\text{SE}} \simeq R_{DC} \ , \ \text{SE} \simeq \eta_0 \frac{\sigma \sinh(\gamma h)}{2\gamma} \simeq 60\pi\sigma h \tag{22}$$

B. Numerical results

First, we find the Shielding Effectiveness (SE) for an infinite aluminum planar slab with a conductivity $\sigma = 3.456 \cdot 10^7$ S/m and a thickness th $= 0.3$ mm under plane-wave incidence. A uniform spatial mesh with $\Delta = 2.5$ mm is used for the free space, and a Gaussian pulse for the excitation with -3 dB decay in amplitude at 1 GHz ($f(t) = e^{-(t-t_0)^2/w^2}$, $t_0 = 0.696$ ns, $w = 0.187$ ns.). Results for a 56^{th} order DigFilt and several SGBC are shown in Fig. 7. As expected, the stability condition, even for the 40-layers case does not need any reduction compared to the usual 3D-FDTD one. We have also included, for reference, results found with the classical Maloney approach [8], which is a type of 1-layer SGBC with extra degrees of freedom to account for the electric field's normal components at the interface (the latter do not have any influence on this problem due to the assumption of normal propagation inside the slab). As expected, Maloney's method fails to catch the skin-depth effect, because of its assumption of constant field inside the slab.

Fig. 8 also presents results for the field at the center of a conductive sphere of radius 1m with a conductivity $\sigma = 200$ S/m and a thickness th $= 5$ mm under the same plane-wave incidence used above. Analytical results from [32] are used for comparison. It bears noting that this problem is far more sensitive to modeling errors than the slab one, and that accurate results are obtained.

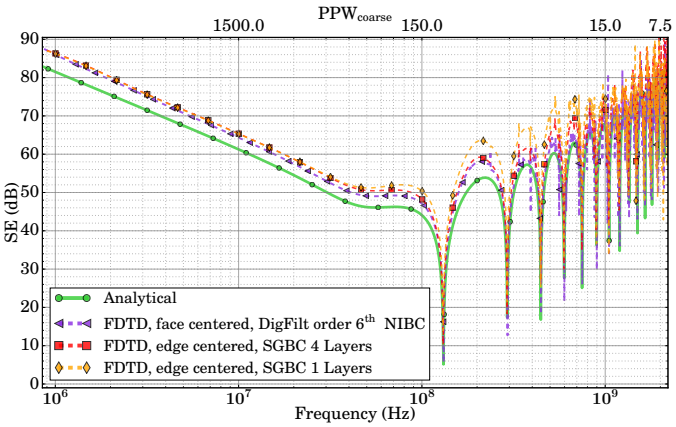

Fig. 8. SE for a sphere of radius 1 m, 200 S/m conductivity and 5 mm thickness.

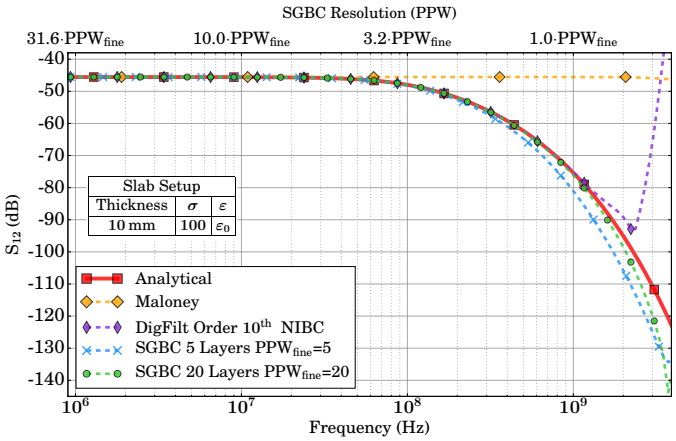

Fig. 9. $S_{12} = \mathrm{SE}^{-1}$ for an infinite homogeneous planar slab, with $\sigma = 100\,\mathrm{S/m}$, and thickness th $= 10\,\mathrm{mm}$. Space step $\Delta_{\mathrm{coarse}} = 20\,\mathrm{mm}$.

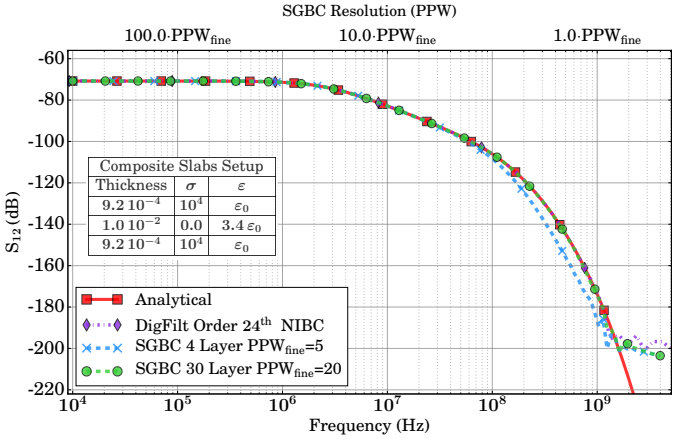

Fig. 10. $S_{12} = \mathrm{SE}^{-1}$ for an infinite 3-layer planar slab. Space step $\Delta_{\mathrm{coarse}} = 20mm$.

Another test case representative of a low conductivity material has been simulated, also under plane wave incidence. The slab has a constant conductivity of $10^4\,\mathrm{S/m}$ and a thickness of $10\,\mathrm{mm}$. The results are shown in Fig. 9. A three-layer slab has also been simulated, with outer layers having $\sigma = 10^4\,\mathrm{S/m}$ and a thickness of $0.92\,\mathrm{mm}$ and the middle one being a lossless thick material of $10\,\mathrm{mm}$ (mimicking a low-density honeycomb). Results are shown in Fig. 10. It bears noting for all the test cases above, that even resolutions inside the slab below 10 cells/wavelength are enough to achieve good results.

Lastly, a final case has been simulated to test the accuracy for LF resistance prediction. A low-conductivity strip with $\sigma = 20\,\mathrm{S/m}$, length $l = 216\,\mathrm{mm}$, width $w = 120\,\mathrm{mm}$, and thickness $h = 2\,\mathrm{mm}$ has been connected at each end to an external U-shaped set of PEC strips (Fig. 11) and excited by a hard voltage delta-gap source. A uniform spatial mesh with $\Delta = 6\,\mathrm{mm}$ is used for the free space, and a quasi-DC source for the excitation, which allows us to get rid of PML conditions and employ PEC ones instead. The current flowing across the material has been calculated and the LF ohmic DC resistance has been found from it and compared to an analytical value of $R_{DC} = \frac{l}{\sigma w h} = 45\,\Omega$.

The vector fitting procedure accurately yields the expected analytical value $Z = Z_\infty + \sum_{k=1}^{P} \frac{r_k}{j\omega - p_k} = \frac{1}{\sigma h} = 25.0\,\Omega$ for all the elements $Z_{i,j}$ of the Z-matrix (3). However, an error in R_{DC} around of 5% was found by DigFilt, whereas for SGBC the error was always under $10^{-3}\%$ as reflected in Table II. The reason for this is the naturally more accurate manner used by SGBC to handle material interfaces by means of the integral versions of Maxwell's equations, and the use of effective values (10) at the interfaces.

V. Conclusions

This paper presents a novel technique for the modeling of thin-layer lossy materials. The approach is demonstrated to be stable and accurate for LF conduction problems, as well as for transmission/reflection ones, this wideband applicability being its main advantage.

We show that the CNTD hybrid provides an accurate scheme for materials arbitrarily thinner than the space step (and even for thicker ones), regardless of the skin-depth of signals involved It does not require reductions in the time step for stability with respect to the usual CFLN in 3D, with low global computational overburden compared to NIBC, and with superior late-time stability properties.

We can summarize some advantages and disadvantages of the SGBC technique compared to the VF NIBC, when dealing with lossy thin-panel materials:

1) The NIBC enables us to deal with thin-panel materials with arbitrary dispersive behavior, as long as the scattering parameters under plane-wave incidence are

TABLE II
Errors in DC prediction of a ($\sigma = 20\,\mathrm{S/m}$), 216 mm long x 120 mm width x 2 mm thick meshed with $\Delta_{\mathrm{coarse}} = 6$ mm.

Method	Error in R_{DC}
Pure Maloney	$< 10^{-3}\%$
SGBC 1 layers	$1.17\,10^{-4}\%$
SGBC 4 layers	$9.62\,10^{-5}\%$
DigFilt NIBC	5.294%

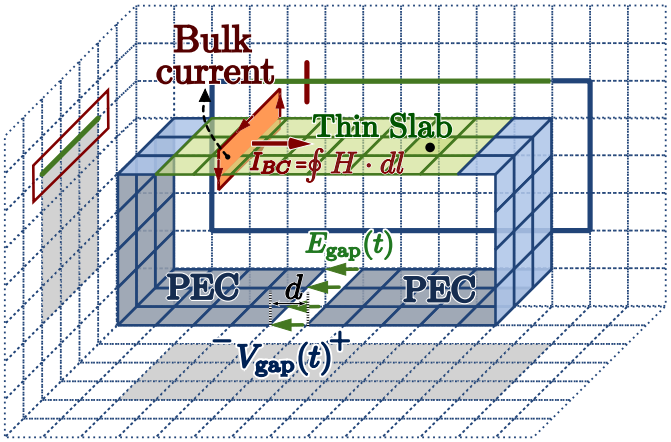

Fig. 11. Test-setup for DC resistance computation.

known either analytically, numerically or experimentally. The SGBC, in principle, requires knowledge of the internal structure of the thin-panel (thickness and bulk conductivity) in order to model wave propagation across it. However, the method can be easily extended for arbitrary frequency dispersion.

2) The NIBC can handle either isotropic and anisotropic panels, whereas the SGBC is affordable only by the use of CNTD in 1D. Unconditionally stable, split-step methods could be used instead to build a 2D anisotropic SGBC.
3) The NIBC exhibits late-time instabilities often difficult to control even by dramatic reductions of CFLN, this is often blamed on the non co-location of the electric and magnetic field components at the surface of the slab. The SGBC employs the natural co-location of Yee-FDTD and does not require reductions with respect to the usual stability limit thanks to the Crank-Nicolson unconditional stability.
4) The NIBC is less accurate than the SGBC to accurately predict the low-frequency resistive behavior of thin-panels, because of modeling errors occurring at material discontinuities. Average parameter methods found from the integral forms of Maxwell's equations, are better suited for it. The SGBC straightforwardly uses this approach at the interfaces, overcoming this limitation in a natural manner.

Appendix A
CNTD coefficients

$$\begin{aligned} a_i &= \left(-\frac{C_{b,i}D_{b,i-1/2}}{4}\right) \\ b_i &= (1-a_i-c_i) \\ c_i &= \left(-\frac{C_{b,i}D_{b,i+1/2}}{4}\right) \end{aligned} \tag{23a}$$

$$a_1 = 0 \quad c_{N+1} = 0 \tag{23b}$$

$$\begin{aligned} d_i^n &= \left(\frac{C_{b,i}}{2}\right)\left(1+D_{a,i-1/2}\right)H_{L,i-1/2}^n \\ &- \left(\frac{C_{b,i}}{2}\right)\left(1+D_{a,i+1/2}\right)H_{L,i+1/2}^n \\ &+ \left(\frac{C_{b,i}D_{b,i-1/2}}{4}\right)E_{L(i-1)}^n \\ &+ \left(C_{a,i} - \frac{C_{b,i}\left(D_{b,i-1/2}+D_{b,i+1/2}\right)}{4}\right)E_{L,i}^n \\ &+ \left(\frac{C_{b,i}D_{b,i+1/2}}{4}\right)E_{L,i+1}^n \end{aligned} \tag{23c}$$

$$\begin{aligned} d_1 &= \left(C_{a,1} - \frac{C_{b,1}D_{b,3/2}}{4}\right)E_{L,1}^n + \left(\frac{C_{b,1}D_{b,3/2}}{4}\right)E_{L,2}^n \\ &+ C_{b,1}\left(H_{S1}^{n+1/2} - \frac{\left(1+D_{a,3/2}\right)}{2}H_{L,3/2}^n\right) \end{aligned} \tag{23d}$$

$$\begin{aligned} d_{N+1} &= \left(C_{a,N+1} - \frac{C_{b,N+1}D_{b,N+1/2}}{4}\right)E_{L,N+1}^n \\ &+ \left(\frac{C_{b,N+1}D_{b,N+1/2}}{4}\right)E_{L,N}^n \\ &+ C_{b,N+1}\left(\frac{\left(1+D_{a,N+1/2}\right)}{2}H_{L,N+1/2}^n - H_{S2}^{n+1/2}\right) \end{aligned} \tag{23e}$$

$$[M] = \begin{pmatrix} b_1 & c_1 & 0 & \cdots & \cdots & 0 \\ a_2 & b_2 & c_2 & \ddots & & \vdots \\ 0 & a_i & b_i & c_i & \ddots & \vdots \\ \vdots & \ddots & & \ddots & & 0 \\ \vdots & & \ddots & a_N & b_N & c_N \\ 0 & \cdots & \cdots & 0 & a_{(N+1)} & b_{(N+1)} \end{pmatrix} \tag{24}$$

$$[E] = \begin{pmatrix} E_{L,1}^{n+1} \\ \vdots \\ E_{L,i}^{n+1} \\ \vdots \\ E_{L,(N+1)}^{n+1} \end{pmatrix}, \; [d]^n = \begin{pmatrix} d_1^n \\ \vdots \\ d_i^n \\ \vdots \\ d_{N+1}^n \end{pmatrix}$$

Acknowledgments

We want to thank Dr. Linda Dawson from the Univ. of York, for her careful proofreading of this manuscript.

References

[1] C. Holloway, M. Sarto, and M. Johansson, "Analyzing carbon-fiber composite materials with equivalent-layer models," *IEEE Trans. Electromagn. Compat.*, vol. 47, no. 4, pp. 833–844, Nov 2005.
[2] M. S. Sarto, S. Greco, and A. Tamburrano, "Shielding effectiveness of protective metallic wire meshes: Em modeling and validation," *IEEE Trans. Electromagn. Compat.*, vol. 56, no. 3, pp. 615–621, June 2014.

[3] I. M. D. Rosa, F. Sarasini, M. S. Sarto, and A. Tamburrano, "Emc impact of advanced carbon fiber/carbon nanotube reinforced composites for next-generation aerospace applications," *IEEE Trans. Electromagn. Compat.*, vol. 50, no. 3, pp. 556–563, Aug 2008.

[4] V. Nayyeri, M. Soleimani, and O. Ramahi, "Modeling graphene in the finite-difference time-domain method using a surface boundary condition," *IEEE Trans. Antennas Propag.*, vol. 61, no. 8, pp. 4176–4182, Aug 2013.

[5] J. Avloni, M. Ouyang, L. Florio, A. R. Henn, and A. Sparavigna, "Shielding effectiveness evaluation of metallized and polypyrrole-coated fabrics," *Journal of Thermoplastic Composite Materials*, vol. 20, no. 3, pp. 241–254, May 2007.

[6] I. Flintoft, J. Dawson, R. Xia, S. Porter, and A. Marvin, "Simulation of materials and joints in FDTD using digital filter macro-models," in *Proc. European Electromagnetics (EUROEM)*, 2012, p. 186.

[7] K. Yee, "Numerical solution of initial boundary value problems involving Maxwell's equations in isotropic media," *IEEE Trans. Antennas Propag.*, vol. 14, no. 3, pp. 302–307, May 1966.

[8] J. Maloney and G. Smith, "The efficient modeling of thin material sheets in the finite-difference time-domain (FDTD) method," *IEEE Trans. Antennas Propag.*, vol. 40, no. 3, pp. 323–330, Mar 1992.

[9] M. Karkkainen, "Subcell FDTD modeling of electrically thin dispersive layers," *IEEE Trans. Microw. Theory Techn.*, vol. 51, no. 6, pp. 1774–1780, June 2003.

[10] M. Leontovich, "Investigation of propagation of radio waves, part II," *Printing House of the Academy of Sciences, Moscow, USSR*, 1948.

[11] M. Sarto, "A new model for the FDTD analysis of the shielding performances of thin composite structures," *IEEE Trans. Electromagn. Compat.*, vol. 41, no. 4, pp. 298 –306, Nov. 1999.

[12] P. Li, Y. Shi, L. J. Jiang, and H. Bagci, "DGTD analysis of electromagnetic scattering from penetrable conductive objects with IBC," *IEEE Trans. Antennas Propag.*, vol. 63, no. 12, pp. 5686–5697, Dec 2015.

[13] M. Feliziani and S. Cruciani, "FDTD modeling of impedance boundary conditions by equivalent lti circuits," *IEEE Trans. Microw. Theory Techn.*, vol. 60, no. 12, pp. 3656–3666, Dec 2012.

[14] G. Kobidze, "Implementation of collocated surface impedance boundary conditions in FDTD," *IEEE Trans. Antennas Propag.*, vol. 58, no. 7, pp. 2394–2403, July 2010.

[15] S. G. Garcia, A. R. Bretones, B. G. Olmedo, and R. G. Martin, "New trends in FDTD methods in computational electrodynamics: Unconditionally stable schemes," in *Recent Res. Development in Electronics*. Transworld Research Network, 2005.

[16] M. Cabello, L. Angulo, A. R. Bretones, R. G. Martin, S. G. Garcia, and J. Alvarez, "A new FDTD subgridding boundary condition for FDTD subcell lossy thin-layer modeling," in *IEEE International Symposium on Antennas and Propagation and CNC/USNC/URSI Radio Science Meeting*, 2010.

[17] J. Wang, B. Zhou, L. Shi, C. Gao, and B. Chen, "A novel 3-D HIE-FDTD method with one-step leapfrog scheme," *IEEE Trans. Microw. Theory Techn.*, vol. 62, no. 6, pp. 1275–1283, June 2014.

[18] D. Frickey, "Conversions between S, Z, Y, H, ABCD, and T parameters which are valid for complex source and load impedances," *IEEE Trans. Microw. Theory Techn.*, vol. 42, no. 2, pp. 205–211, Feb. 1994.

[19] B. Gustavsen and A. Semlyen, "Rational approximation of frequency domain responses by vector fitting," *IEEE Trans. Power Del.*, vol. 14, no. 3, pp. 1052 –1061, jul 1999.

[20] M. C. O. Jansson, S. P. O. Ljung, M. G. Backstrom, and B. I. Wahlgren, "Efficient implementation of a submodel for composite materials to be combined with the fdtd-algorithm," *IEEE Trans. Magn.*, vol. 30, no. 5, pp. 3188–3191, Sep 1994.

[21] M. White, M. Iskander, and Z. Huang, "Development of a multigrid FDTD code for three-dimensional applications," *IEEE Trans. Antennas Propag.*, vol. 45, no. 10, pp. 1512–1517, Oct 1997.

[22] A. Taflove and S. C. Hagness, *Computational Electrodynamics The Finite-Differences Time Domain Method*. Artech House, 2005.

[23] M. D'Amore and M. S. Sarto, "Time domain analysis of lightning interactions to aeronautical structures composite materials," in *IEEE Int. EMC Symp.*, Austin, TX, Aug. 1997, pp. 397–402.

[24] S. G. Garcia, T.-W. Lee, and S. Hagness, "On the accuracy of the ADI-FDTD method," *IEEE Antennas Wireless Propag. Lett.*, vol. 1, no. 1, pp. 31–34, 2002.

[25] H. Rouf, F. Costen, and S. G. Garcia, "3D crank-nicolson finite difference time domain method for dispersive media," *Electronics Letters*, vol. 45, no. 19, pp. 961–962, September 2009.

[26] C. Schuster, A. Christ, and W. Fichtner, "Review of FDTD time-stepping schemes for efficient simulation of electric conductive media," *Microw. Opt. Technol. Letters*, vol. Vol. 25, pp. 16–21, 2000.

[27] X. Chen, T. M. Grzegorczyk, B.-I. Wu, J. Pacheco, and J. A. Kong, "Robust method to retrieve the constitutive effective parameters of metamaterials," *Phys. Rev. E*, vol. 70, p. 016608, Jul 2004.

[28] M. Han, R. Dutton, and S. Fan, "Model dispersive media in finite-difference time-domain method with complex-conjugate pole-residue pairs," *IEEE Microw. Compon. Lett.*, vol. 16, no. 3, pp. 119 –121, March 2006.

[29] S. G. Garcia, R. Rubio, A. Bretones, and R. Martin, "On the dispersion relation of ADI-FDTD," *IEEE Microw. Compon. Lett.*, vol. 16, no. 6, pp. 354–356, June 2006.

[30] S. Wang, F. L. Teixeira, R. Lee, and J.-F. Lee, "Optimization of subgridding schemes for FDTD," *IEEE Microw. Compon. Lett.*, vol. 12, no. 6, pp. 223–225, June 2002.

[31] W. Yu, X. Yang, Y. Liu, R. Mittra, and A. Muto, *Advanced FDTD Methods (Parallelization, Acceleration, and Engineering Applications)*. Artech House, 2011.

[32] F. M. Tesche, "Electromagnetic field shielding of a spherical shell–revisited," *Forum for Electromagnetic Research Methods and Application Technologies*, vol. 3, 5-6 2014. [Online]. Available: http://www.e-fermat.org/files/articles/1536cfedc80f6b.pdf

[33] G. Singh, E. L. Tan, and Z. N. Chen, "A split-step FDTD method for 3-d maxwell's equations in general anisotropic media," *IEEE Trans. Antennas Propag.*, vol. 58, no. 11, pp. 3647–3657, Nov. 2010.